Modelling of an industrial moving belt chemical vapour deposition reactor forming SiO_2 films

J.P. Nieto[a], L. Jeannerot[b], B. Caussat[c,*]

[a]*ASML Thermal Division, 100 Allée Saint Exupéry, 38330 Montbonnot, France*
[b]*ATMEL, ZI Peynier Rousset, 13000 Rousset, France*
[c]*LGC/ENSIACET/INPT, BP1301, 5 rue Paulin Talabot, 31106 Toulouse Cedex 1, France*

Abstract

In order to improve the efficiency of an industrial atmospheric pressure chemical vapour deposition (APCVD) moving belt reactor depositing silicon dioxide SiO_2 films from tetraethoxysilane $Si(OC_2H_5)_4$ (TEOS) and ozone O_3, a 2D simulation model based on the computational fluid dynamics (CFD) software ESTET has been developed.

On the basis of the global chemical scheme of Zhou et al. [1997. Fifth International Conference on Advanced Thermal Processing of Semiconductors, RTP'97, New Orleans, LA, USA, pp. 257–268], a new kinetic model has been developed to conveniently represent our own set of experimental data. In particular, a chemical limitation for TEOS has been introduced, conferring increased chemical validity to the model. Simulations have shown that for the nominal conditions, TEOS conversion into SiO_2 layers was too low and that an increase in ozone concentration or in the nitrogen flow rates through the injector did not offer any advantage. Conversely, a decrease in the curtain nitrogen flow rate or an increase in that of the shield can enhance the process productivity and TEOS conversion.

Keywords: CVD; Modelling; Silicon dioxide; Electronic materials; Multiphase reactions; Process optimization

1. Introduction

Doped or undoped silicon dioxide films are commonly used as premetal or interlevel dielectric layers in the integrated circuit industry (Saito et al., 2003). These films are increasingly processed by atmospheric pressure chemical vapour deposition (APCVD) from tetraethoxysilane, $Si(OC_2H_5)_4$ (TEOS) and ozone O_3 mixtures, because this route offers clear advantages over the conventional silane-oxygen process. In particular, step coverage is improved, deposition temperature lowered ($< 550\,^{\circ}C$) and the contamination level due to in situ powdering suppressed (Fujino et al., 1990; Yuan et al., 1996; Adachi et al., 1997; Okuyama et al., 1997; Zhou et al., 1997). The advantages of TEOS over monosilane are safety, ease of handling and chemical stability (Fujino et al., 1990). Operating at atmospheric pressure also presents some marked advantages over more conventional low pressure CVD processes: (i) the absence of vacuum conditions decreases the technological complexity, and hence the production costs, (ii) the deposition rate is much higher than for low pressure (LP) technologies, greater than $100\,nm\,min^{-1}$, (iii) wafers can then be processed continuously, the slices being placed on a belt circulating through successive deposition chambers (Masi et al., 1997). This leads to higher productivities as compared to batch reactors.

However, very often film uniformity on each wafer and from wafer to wafer as well as the process throughput rate could be improved regarding industrial specifications. This last point constitutes a non-negligible problem since the cost of TEOS represents a large contribution to the total cost of the operation (Dobkin et al., 1995). Phenomena occurring in APCVD equipments are complex, because convective

* Corresponding author. Tel.: +33 5 34 61 52 11; fax: +33 5 34 61 52 53.
E-mail address: Brigitte.Caussat@ensiacet.fr (B. Caussat).

momentum transfers are tightly coupled with both thermal profiles, presenting sharp thermal gradients, and with mass transfer phenomena, including numerous homogeneous and heterogeneous chemical reactions. Indeed, TEOS is a quite complex organosilicon molecule. When placed in a highly oxidative medium such as O_3, numerous chemical reactions take place in the gas phase and on surfaces. Optimizing such a complex process purely experimentally would necessitate numerous and costly experiments. Undoubtedly, the determination of the operating conditions leading to high process efficiency and high-quality films can be facilitated and accelerated using computational fluid dynamics (CFD) (Coltrin et al., 2000). But certainly because of their novelty, APCVD processes have been the object of far fewer numerical and even experimental studies than the older LP CVD processes (Nieto, 2001).

The aim of the present work is then to contribute to this effort by using CFD to analyse the influence of the main operating parameters on the process behaviour to improve its general efficiency, in terms of productivity and of TEOS conversion.

2. The APCVD reactor and the experimental data

The silicon oxide films studied were deposited in an industrial APCVD Watkins Johnson WJ1000 system, from TEOS, ozone and oxygen mixtures highly diluted in nitrogen. As illustrated in Fig. 1a, the reactor consists of a muffle containing four deposition chambers separated from each other by nitrogen curtains. Wafers of 200 mm diameter are horizontally transported through the muffle by a continuously moving belt cleaned in a hydrofluoric acid (HF) vapour bath after unloading the wafers. The belt is made of Inconel 601, an alloy resisting the action of HF and presenting a high thermal conductivity, to ensure uniform thermal profiles along the muffle. Nitrogen curtains near the open ends of the reactor prevent entry of ambient air.

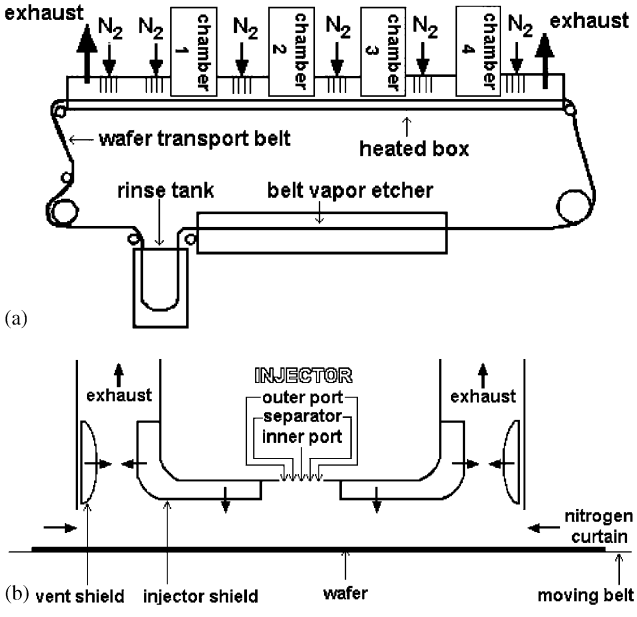

Fig. 1. (a) Schematic representation of the industrial APCVD reactor; (b) detail of one deposition chamber.

In each chamber, a gas injector delivers three different gas mixtures, organized into five thin sheaths as shown in Fig. 1b. The centre channel (inner port) dispenses TEOS diluted in nitrogen; the intermediate channels (separator ports) deliver pure nitrogen, and the two outermost sheaths (outer ports) dispense ozone and oxygen diluted in nitrogen. Gas fluxes were uniform along the width of the deposition chamber. Each injector is water cooled and was maintained at a temperature of around 70 °C, essentially to prevent premature chemical reactions from occurring. Nitrogen was also injected through the injector and vent shields, as can be seen in Fig. 1b, in order to limit parasitic deposition in these zones. Experimental measurements have shown that the temperature of the shields was about 400 °C. The heater settings were adjusted through 75 independent elements divided into three zones along the reactor muffle, to produce a thermal gradient from 500 °C on the wafer surface beneath the gas injector, increasing linearly to 520 °C near the nitrogen curtain. TEOS being in a liquid state at ambient pressure and temperature, its gas flow is produced by a conventional temperature-controlled nitrogen bubbler maintained at 65 °C. The ozone flow is obtained by passing oxygen through a Sumitomo ozonator producing gaseous oxygen/ozone mixtures. The ozone concentration in these mixtures was measured by an in-line UV photometer.

All deposition experiments were performed in static mode (i.e., the wafer remaining motionless and centred exactly under the injector), in order to develop and then validate the numerical model. The deposit thickness was measured along the wafer diameter corresponding to the moving belt axis by profilometry using a Tencor Prometrix UV1280SE.

The operating conditions tested are presented in Table 1. For all experiments, run duration was fixed at 4 min.

First, the reproducibility in terms of deposition rate was studied by performing four identical experiments in the conditions of the nominal run, referred to as S1 in Table 1. This series of experiments was used to evaluate the reproducibility of deposition and hence determine a reasonable precision for the numerical model results. The dispersion of the experimental results was not negligible, since under the injector, a maximum deviation of 7.5% was observed, whereas at 30 mm from the injector axis, deviation reached 30%. This rather high value shows how the fine tuning of this process is difficult to perform and to maintain due to the strong interconnections existing between the momentum, heat and reactive mass transfer parameters. Consequently, it was arbitrarily decided that the model results were in agreement with experiment when the difference between the two was lower than 10%.

Table 1
Experimental operating conditions

Run	T (°C)	N_2 flow rate into the TEOS bubbler (lpm)[a]	N_2 flow rate in the inner port of the injector (lpm)	TEOS flow rate (sccm)[b]	N_2 flow rate in the separator port (lpm)	O_2 and O_3 flow rate (lpm)	O_3 concentration ($g\,m^{-3}$)
S1	500	1.695	3.615	40.3	9	7	125
S2	500	1	4.31	23.8	9	7	125
S3	500	0.5	4.81	11.9	9	7	125
S4	500	1.695	3.615	40.3	2.25	7	125
S5	500	1.695	3.615	40.3	12.75	7	125
S6	500	1.695	3.615	40.3	9	7	100
S7	500	1.695	3.615	40.3	9	7	139

[a]Litres per minute STP.
[b]Standard cubic centimetres per minute.

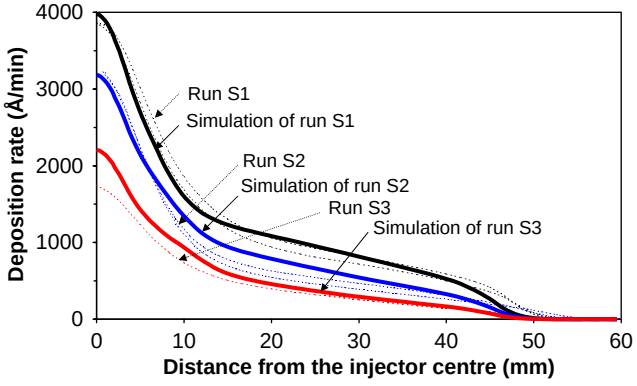

Fig. 2. Experimental deposition rate profiles obtained for different TEOS flow rates (runs S1 to S3) and comparison with simulations.

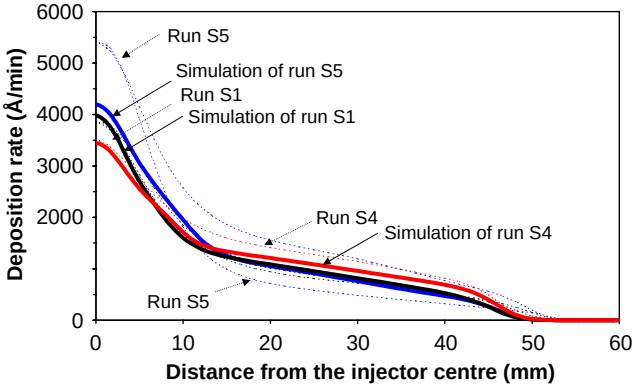

Fig. 3. Experimental deposition rate profiles obtained for different SepN2 flow rates (runs S1, S4, S5) and comparison with simulations.

The influence of TEOS flow rate was analysed through runs S1–S3. Runs S2 and S3 were performed twice. All the results are presented in Fig. 2. It appears that the TEOS inlet partial pressure plays an important role in the process, since its increase directly enhances the deposition rates throughout the deposition chamber.

The nitrogen flow rate in the separator port (SepN2) was then studied through runs S4 and S5, each experiment being performed twice, as represented in Fig. 3. These runs allowed the influence of the total inlet gas flow to be analysed without modifying the precursor flow rates.

It can be observed that an increase in SepN2 enhanced the deposition rate mainly under the injector. This behaviour is in perfect agreement with the claims of Watkins Johnson Co. Ltd. (Watkins Johnson, 1997). In contrast, results obtained for run S6 are more surprising since a decrease in SepN2 had no effect. Unfortunately, this run could not be repeated for production reasons; this particular result must then be considered with care.

The ozone flow rate was varied through runs S6 and S7 modifying only the ozone concentration by acting on the electric power supplied to the ozonator. As can be seen in

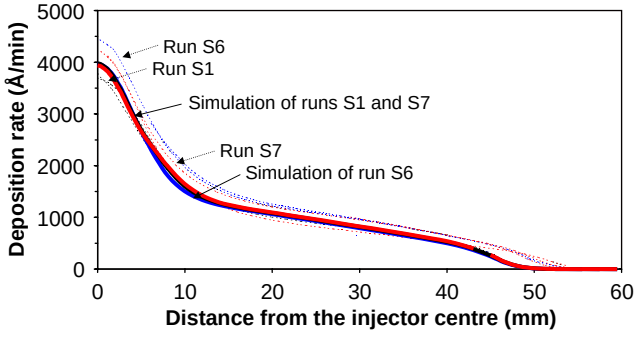

Fig. 4. Experimental deposition rate profiles obtained for different ozone concentrations (runs S1, S6, S7) and comparison with simulations.

Fig. 4, a weak influence was observed along the deposition chamber. This behaviour is not surprising since in the conditions tested, the molar ratio of the O_3 and TEOS inlet concentrations was varied between 8.1 and 11.2, i.e., there was always a large excess of ozone. This result is similar to that obtained by Kotani et al. (1989) for which O_3 exerts an important influence only when the O_3/TEOS ratio remains

low. Such high ratio is recommended in this process because it limits the carbon or hydrogen contamination of deposits (Nieto, 2001).

3. The numerical model of reactor

As previously mentioned, the phenomena involved in the TEOS/ozone APCVD process include tightly coupled fluid flow, heat transfer, mass transport of multiple gas species and chemical reactions in the gas phase and on surfaces of the reactive zone. As a consequence, a numerical model for this process involves partial differential equations describing the conservation of mass, momentum, energy and chemical species, associated to appropriate boundary conditions.

The CFD code ESTET (Ensemble de Simulations Tridimensionnelles d'Ecoulements Turbulents) developed by EDF (Electricité De France) and distributed by Simulog (http://www.simulog.fr/eis/2estet1.htm) was used in this work.

Some reasonable simplifying assumptions have been applied to reduce the complexity of the numerical problem:

- The steady state regime is assumed.
- Gas flow is incompressible (Mach number much lower than 0.4) and laminar (Reynolds number is about 100).
- The reactive gases being highly diluted in nitrogen, the gas mixture is ideal, and energy contribution due to chemical reactions negligible.
- For reasons of symmetry, only half a single chamber and one wafer radius along the chamber axis was considered.
- The belt and wafers are assumed motionless, since their velocity is far lower than that of the gases. The wafer is assumed to be centred under the injector.

On the basis of these assumptions, the 2D geometrical domain studied is given in Fig. 5. It corresponds to half of a gas injector, the nitrogen shields and the side curtain, and a half diameter of wafer. This domain involves 130 × 26 structured meshes in a half-staggered grid.

The associated boundary conditions are as follows:

- At the inlet, a flat profile is imposed on the gas velocity; the gas feed is assumed to be at a temperature of 70 °C; the gaseous mass fractions in each region of the injector are fixed at the experimental values (Dirichlet condition).
- At the curtain and shields, a flat profile is imposed for gas velocity and nitrogen is assumed to enter at a temperature of 70 °C; the surface temperature of the shields is fixed to 400 °C; the mass flux density for each species is assumed to be equal to the corresponding heterogeneous reaction rate on the shield surface.
- On the wafer surface, a classical no slip condition for gas velocity is applied; the temperature is assumed to increase linearly from 500 °C at the symmetry axis to 520 °C near the nitrogen curtain; each species mass flux density is assumed to be equal to the corresponding heterogeneous reaction rate.
- At the exit (exhaust), the total pressure is fixed at 1 atm, and Danckwerts conditions (diffusive flux density equal to zero) are imposed for gas velocity, temperature and mass fractions.
- At the lateral plane of symmetry, these Danckwerts conditions are also applied for gas pressure, velocity, temperature and mass fractions.

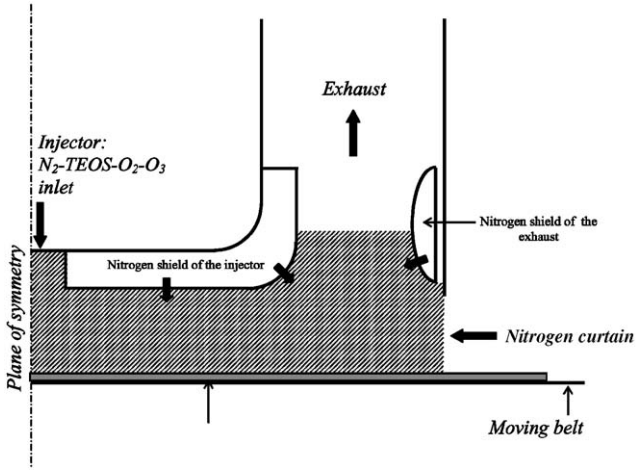

Fig. 5. The geometrical modelling domain studied.

The physical properties of the gaseous mixture were calculated from classical correlations in the literature, Hirschfelder et al. (1954) for dynamic viscosity and for thermal conductivity and Chapman and Enskog (Reid et al., 1987) for molecular diffusivity.

Furthermore, a major result given by modelling is the deposition rate, usually expressed in Angstroem per minute to be compared to experimental values. To convert the molar flux density of deposited species given by the model in this industrial unit, the SiO_2 deposits were taken to have a density of 2200 kg m^{-3}, as recommended by Kim (1993).

4. Development of the kinetic model

4.1. TEOS/O_3 chemical mechanisms

Kim and Gill (1994) were the first to study the TEOS/O_3 chemistry in a cold wall vertical single-wafer CVD reactor, for an operating range very different from ours, i.e., a temperature between 280 and 405 °C and a total pressure between 30 and 90 Torr. However, their approach is interesting because they were the first to develop a global apparent mechanism, in which the various species formed from homogeneous TEOS decomposition are considered through a single fictive molecule named INT. Once formed, this INT species can then either decompose into parasitic gaseous

Table 2
The chemical model of Zhou et al. (1997)

		Reaction step	Reaction rate
Homogeneous reactions ($kmol\,m^{-3}\,s^{-1}$)	(R1)	$O_3 + M \rightarrow O_2 + O + M$	$k1\ [O_3][M]$
	(R2)	$O_3 + O \rightarrow 2O_2$	$k2\ [O_3][O]$
	(R3)	$2O + M \rightarrow O_2 + M$	$k3\ [O]^2[M]$
	(R4)	$O_3 + TEOS + M \rightarrow INT + R + M$	$k4\ [O_3][TEOS][M]$
	(R5)	$INT \rightarrow$ by-products	$k5\ [INT]$
Surface reactions ($kmol\,m^{-2}\,s^{-1}$)	(R6)	$TEOS + 6O_3 \rightarrow SiO_2(s) + O_2 +$ by-products	$k6\ [TEOS]_s^m[O_3]_s^n$
	(R7)	$INT \rightarrow SiO_2(s) +$ by-products	$k7\ [INT]_s/(1 + k8[INT]_s)$

Table 3
Formulation of the various kinetic constants (temperature are in K)

	Zhou et al. (1997)	This work	Units
k_1	$2.5 \times 10^{11} \exp\left(-\frac{11430}{T}\right)$		$m^3\,kmol^{-1}\,s^{-1}$
k_2	$10^{10} \exp\left(-\frac{2090}{T}\right)$		$m^3\,kmol^{-1}\,s^{-1}$
k_3	$4 \times 10^8 \exp\left(+\frac{720}{T}\right)$		$m^6\,kmol^{-2}\,s^{-1}$
k_4	$4 \times 10^{17} \exp\left(-\frac{14099}{T}\right)$		$m^6\,kmol^{-2}\,s^{-1}$
k_5	$10^5 \exp\left(-\frac{5539}{T}\right)$	$5 \times 10^3 \exp\left(-\frac{5539}{T}\right)$	s^{-1}
k_6	200	0.00041	$m^{-0.05}\,kmol^{0.35}\,s^{-1}$
k_7	$20 \exp\left(-\frac{4053}{T_s}\right)$	$1.2 \exp\left(-\frac{4053}{T_s}\right)$	s^{-1}
k_8	$1.14 \times 10^7 \exp\left(-\frac{2578}{T_s}\right)$	$1.482 \times 10^6 \exp\left(-\frac{2578}{T_s}\right)$	$m^3\,kmol^{-1}$
m	1	0.4	—
n	0.25		—

by-products or contribute to SiO_2 deposition. The kinetic laws were fitted from experimental data.

Following a similar approach, Dobkin et al. (1995) and Zhou et al. (1997) then developed their own chemical and kinetic systems to model APCVD Watkins Johnson reactors.

Only the model of Zhou et al. is presented in detail since their experimental conditions are quite close to ours, i.e., a wafer temperature between 500 and 550 °C in a reaction chamber quite similar to that studied in the present work and operating at atmospheric pressure.

The apparent chemical reactions they considered, together with the corresponding kinetic laws are presented in Table 2. M represents the gas mixture and [M] the total gas concentration, the index *s* referring to surface concentrations. Reactions 1–3 correspond to the thermal decomposition of ozone in molecular oxygen and in highly reactive atomic oxygen. Reaction 4 summarizes all the gaseous decomposition routes of TEOS, leading to some unreactive molecules called R and to intermediate compounds called INT; these INT compounds are able to react on surfaces to contribute to deposition. Reaction 5 stands for the degradation of INT in gaseous by-products unable to react on surfaces. It is worth noting that in the range of temperatures considered, experiments have shown that the deposition rate decreases as temperature increases (Dobkin et al., 1995); the role of reaction 5 is to represent all the parasitic reactions responsible for this phenomenon. Reaction 6 expresses the direct contribution of TEOS to the deposit, whereas reaction 7 corresponds to the contribution made by INT molecules. The latter reaction also forms unreactive by-products. The formulation of all the kinetic constants involved is given in Table 3, index S referring to surface temperatures.

4.2. Simulation of the nominal run S1 using the kinetic model of Zhou et al.

The modelling results for the operating conditions of run S1 using the kinetic model of Zhou et al. are presented in Figs. 6 and 7. It can be observed that gas flow can be described as a high speed jet impinging on the wafer surface. Near the surface, a division of this flow into two symmetrical

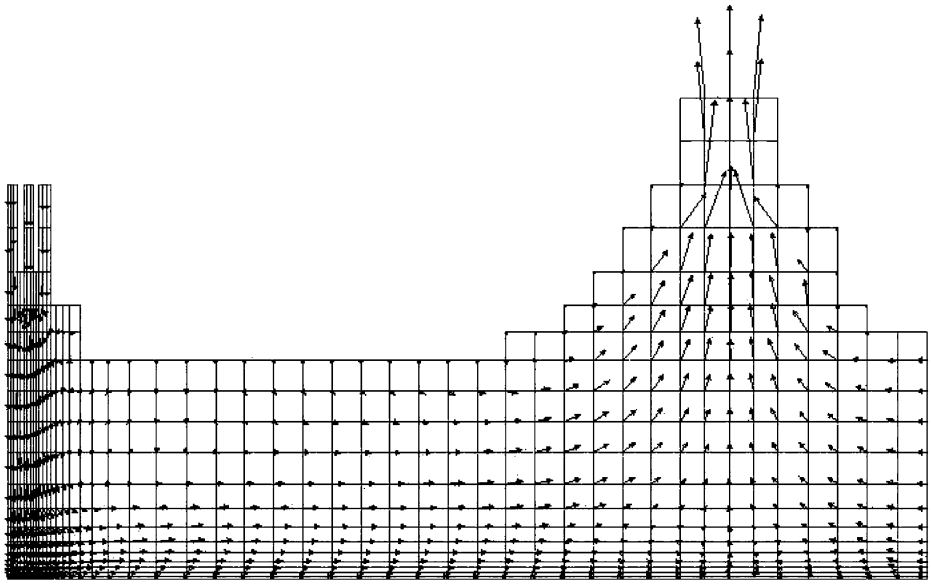

Fig. 6. Simulated gas velocity field for run S1 using the kinetic model of Zhou et al.

parts parallel to the wafer occurs as a result of the assumption of symmetry. The whole gas flow (entering from the injector, shields and curtain) is then gathered together and transferred towards the exhaust zone. It is in this zone that the gas velocity is the highest, $2\,m\,s^{-1}$, whereas it does not exceed $0.5\,m\,s^{-1}$ in the entrance jet.

No recirculation region was observed. However, specific simulations have shown that such regions can appear when the nitrogen flow through the shield is suppressed. The role of the shield is then essential, since recirculation zones would constitute possible sources of undesirable homogeneous nucleation and particle formation.

The temperature field shows that the gas stream from the injector remains cool until it reaches the vicinity of the hot wafer surface, where it increases sharply from 70 to 500 °C. The thermal boundary layer underneath the injector appears very thin, about 3 mm in thickness. The thickness of this hot zone increases along the wafer radius, but the mean gas temperature in the reactor remains about 400 °C.

Concerning the mass fractions of the various species involved, the following features can be mentioned:

- An intense mixing of gas streams occurs in the region between the injector and the wafer, although a complete homogeneity of concentration is not reached near the wafer.
- Ozone and TEOS are rapidly depleted in the 3-mm-thick heated region near the wafer surface, exclusively by gas-phase reactions; this spectacular ozone decomposition gives rise to atomic oxygen responsible for the homogeneous decomposition of TEOS.
- INT species are produced in the intense decomposition zone of TEOS/ozone and then flow along the wafer surface. Their mass fraction then decreases due to surface reactions and parasitic consumption to form by-products, leading to the characteristic bell pattern of the thickness profile, as presented in Fig. 8.
- Only 16.6% of the inlet silicon atoms are converted into SiO_2 deposits; 15.3% are directly evacuated without decomposing at all, 45.6% give INT species and 22.5% lead to by-products. The chemical yield of the operation is then very low. The unconverted silicon species are responsible for unwanted fouling in the exhaust zone, requiring complete cleaning of the process every 35 h.

These results confirm that the possibilities of progress in terms of process optimization are high.

Fig. 8, which compares the experimental and calculated deposition rate profiles, shows a high deposition rate peak under the injector, followed by a plateau spreading more or less along the reaction chamber. But modelling leads to a highly overestimated peak, and to a shorter and weaker plateau. The kinetic model of Zhou et al. is then unable to accurately represent our process.

This failure certainly arises from the fact that Zhou et al. did not consider the influence of the shields, which implies that the temperature field they obtained was quite different from ours. So, we simulated various nitrogen velocity profiles from the shields and the curtain, but no improvement was obtained. The only remaining solution was then to test and recalibrate each kinetic constant of the apparent chemical model of Zhou et al.

4.3. Towards new kinetic laws

Assuming that the peak under the injector was due to the direct contribution of TEOS, whereas the plateau was

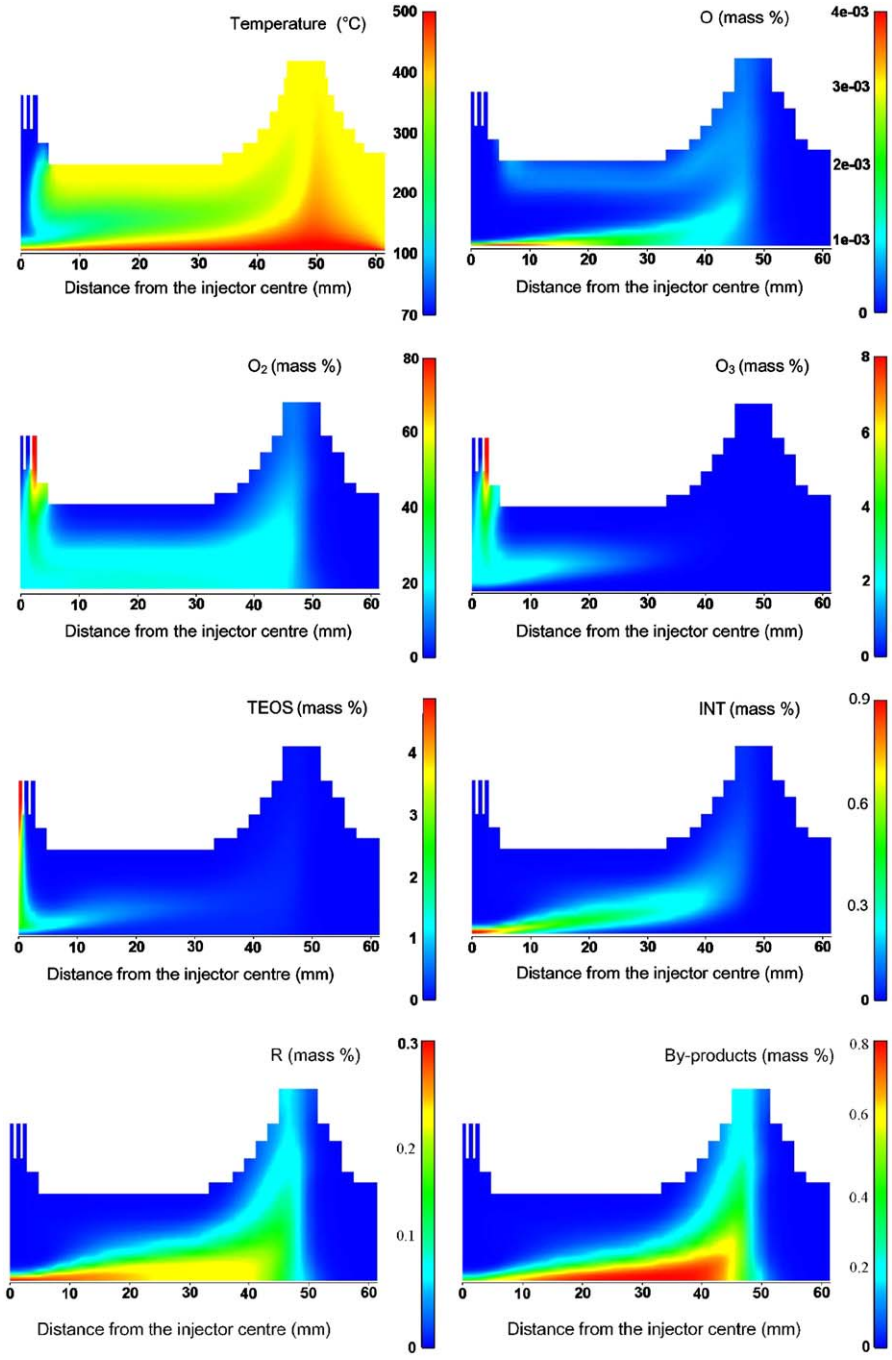

Fig. 7. Simulated temperature and mass fraction maps for run S1 using the kinetic model of Zhou et al.

due to the INT contribution, the kinetic laws were adjusted in two steps: (i) fitting the TEOS peak by modifying constants $k1$, $k2$, $k3$, $k4$ and $k6$, (ii) fitting the INT plateau with constants $k5$, $k7$ and $k8$. Only runs S1–S3 were considered here.

By increasing the values of $k1$ or $k4$, the amount of precursor reaching the surface decreases, which allows the value of the TEOS contribution leading to the peak to be adjusted. The INT plateau can then be modulated: by decreasing the $k5$ constant, the R5 reaction is lowered, and INT is present farther along the deposition chamber. Finally, the $k7$ and $k8$ constants adjust the intensity of the deposit contribution for the INT species.

After several trials, a significant improvement of the model predictions was obtained, but the accuracy of the simulations remained low. Therefore, we strongly decreased constant $k6$ in order to reach chemical limitation instead of transport limitation. Moreover, to definitely refine our results, an exponent of 0.25 was introduced for the TEOS concentration in the R6 law. The final values of our

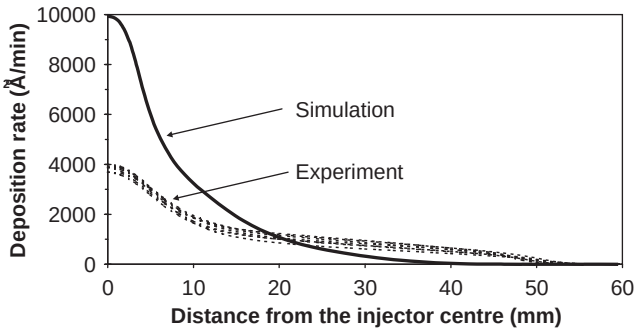

Fig. 8. Comparison between the experimental and calculated deposition rate profiles using the kinetic model of Zhou et al.

kinetic constants are given in Table 3. The corresponding simulation results are presented in Fig. 2.

From a theoretical point of view, the arbitrary introduction of a partial order for TEOS is valid for the essential reason that all the chemical reactions considered in the model are apparent and stand for numerous elementary mechanisms. Moreover, for surface reactions, the apparent kinetic order for a given species may not be equal to the stoichiometric coefficient, since the surface reaction stands for numerous phenomena, such as reactive species adsorption, surface migration, chemical reaction, product desorption. From a chemical point of view, the value for the $k6$ constant chosen by Zhou et al. was so high that the R6 surface reaction was infinitely rapid. This possibility seems hardly realistic for a reaction involving a saturated relatively unreactive species like TEOS. The assumption of a chemical limitation therefore appears much more reasonable.

4.4. Experimental validation of the kinetic model

The model was developed on the basis of three experiments S1–S3, corresponding to three different TEOS flow rates. Simulations of the remaining experimental data are presented in Figs. 3 and 4, for different nitrogen flow rates in the separator (SepN2) and various ozone concentrations.

Let us recall that the experimental data concerning the influence of the SepN2 flow rate are quite contradictory. An enhancement of SepN2 beyond 9 lpm (standard litres per min) produced a strong elevation of the deposition rate, whereas a strong decrease of SepN2 did not notably modify the deposition rate. Simulations show that the influence of SepN2 remains low. A good agreement is obtained for the lowest flow rate experiment S4 and of course for S1.

For O_3 concentration, as shown in Fig. 4, the agreement between experiment and simulation is quite satisfactory even though the experimental deposition rate decreases slightly as the O_3 level increases, whereas the calculated deposition rate remains quite constant.

5. Numerical analysis of the main process parameters influence

To improve the productivity and more generally the exploitation conditions of the process, a systematic analysis of the operating parameters was performed. Indeed, once validated, the main interest of such a predictive model is to simulate various deposition conditions either difficult to test experimentally for safety or availability reasons or technologically impossible to perform due, for instance, to mass flow meter limitations. The parameters numerically investigated here were the TEOS and ozone flow rates, those of nitrogen in the inner, separator and outer ports of the injector, and those of the curtain and shields. For each simulation of this study, the operating parameters were those of the nominal run S1, except for the one actually under investigation which was varied around its nominal value.

5.1. TEOS flow rate

The TEOS flow rate was varied between 11.9 and 95.1 sccm (standard cubic centimetres per min), corresponding to a bubbler nitrogen flow rate of 0.5–4 lpm. The corresponding modelling results are presented in Fig. 9. It clearly appears that the deposition rate increases with the TEOS flow rate. But this elevation tends towards a plateau for the highest flow rates. Saturation then leads to a decrease in TEOS contribution to deposition.

This information is important because the deposition rate can be enhanced by increasing the TEOS flow rate to improve the reactor productivity, but this induces faster fouling of the deposition chamber and of the exhaust. A compromise should be found between the gain in productivity and the cost of equipment maintenance and precursor consumption.

5.2. Ozone concentration

This parameter was varied between 0 and 139 g m^{-3}, the nominal S1 value being fixed at 125 g m^{-3}. Simulation results are presented in Fig. 10. They are in agreement with observations of other authors (Kim and Gill, 1994; Dobkin

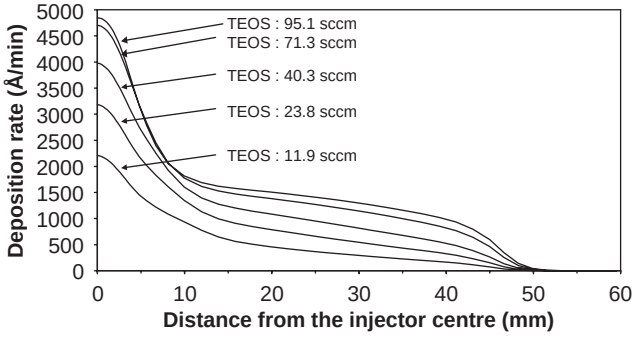

Fig. 9. Influence of TEOS flow rate on deposition rate.

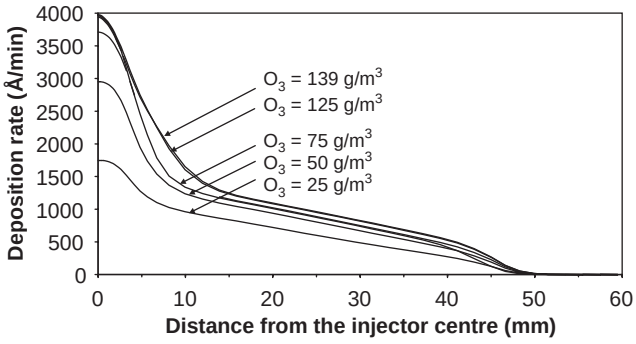

Fig. 10. Influence of ozone concentration on deposition rate.

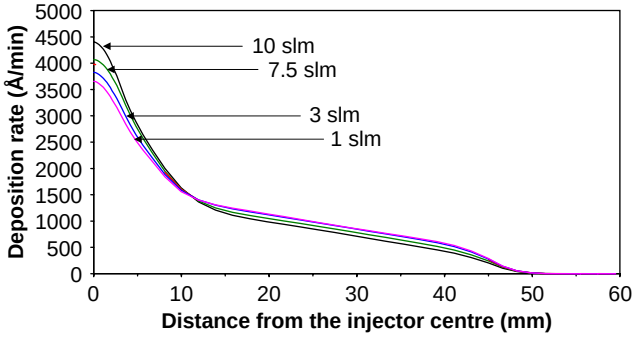

Fig. 11. Influence of nitrogen flow rate in the inner port of the injector on deposition rate.

et al., 1995). They show that the deposition rate is proportional to the O_3 concentration only if this concentration remains low and of the same order of magnitude as that of TEOS. As mentioned in Section 2, beyond 100 g m^{-3}, ozone is in excess near the wafer and the deposition rate becomes independent of it. This suggests that the nominal set up is with an excess of ozone. But this excess is important to ensure the quality of the deposit, in particular concerning its carbon content.

Consequently, neither the productivity of the reactor nor the deposition rates can be improved through the modification of the ozone flow rate.

5.3. Nitrogen flow rate in each zone of the injector

The nitrogen flow rate in the inner port of the injector was varied between 1 and 10 slm, the TEOS flow rate being kept constant at 40.3 sccm. As shown in Fig. 11, the simulation results indicate that when this flow rate is increased, the peak under the injector is higher, whereas the plateau decreases in thickness. The cumulative value in a chamber is then roughly independent of this parameter. The reason for this behaviour is that when the nitrogen flow rate increases, the TEOS residence time in the hot zone near the surface is shorter. As a consequence, the amount of TEOS arriving at the surface is higher and the amount of INT formed is lower.

A similar result was obtained by varying the nitrogen flow rates in the separator and outer zones of the injector. No significant improvement was then obtained, through an evolution of these parameters.

5.4. Nitrogen flow rate in the curtain and the shield

The nitrogen flow rate of the shield was varied between 0 and 40 lpm, the nominal value being 20 lpm. Results show that this parameter did not influence the deposition rate under the injector, whereas its enhancement increased the deposition rate for the last 30 mm of the wafer radius. The reason is that the deposition rate below the injector is hydrodynamically controlled by the injector flow rate. Therefore, whatever the shield flow rate, the residence time of O_3 and TEOS in the hot zone near the surface is the same, so the TEOS peak and the amount of INT formed under the injector are identical. But raising the shield N_2 flow rate favours contact between the INT vein and the wafer. Thus the (R7) reaction is enhanced and the deposition rate increased. This result is important since it leads to the idea that a new design of this part of the shield could bring the INT vein significantly nearer the wafer so as to increase the TEOS conversion yield.

Lastly the nitrogen flow rate of the curtain was varied between 0 and 30 lpm. The results indicate that the action of this parameter only concerns the region between 40 and 60 mm from the injector centre, i.e., the part of the wafer very close to the curtain. In fact, when the curtain flow rate decreases, the INT species can go further in the reaction chamber and even occupy the whole chamber width when the curtain flow rate is zero. The R7 reaction can then logically concern a larger zone near the curtain. However, this parameter must not be lowered too much, because contamination due to ambient dust or entry of air could appear.

6. Conclusions

A new 2D model based on the CFD software ESTET has been developed to study an Atmospheric Pressure Chemical Vapour Deposition moving belt reactor depositing SiO_2 film from tetraethoxysilane $Si(OC_2H_5)_4$ (TEOS) and ozone O_3. We have shown that for the nominal operating conditions, TEOS conversion into SiO_2 films was very low, inducing both rapid fouling of the exhaust zone and waste of the costly TEOS precursor. At the same time, ozone is rapidly and totally consumed under the injector and no advantage is to be gained from increasing its concentration. The global chemical scheme of Zhou et al. (1997) has been retained, but their kinetic constants had to be modified in order to conveniently represent our own set of experimental data. In particular, a chemical limitation for TEOS has been introduced, thus conferring an increased chemical validity to the model.

It is now established that varying the ozone concentration or nitrogen flow rates in the various parts of the

injector cannot improve the process performance. An increase in the TEOS flow rate enhances the deposition rate but lowers the TEOS conversion, and so favours fouling of the exhaust. However, the important role of the shield nitrogen flow in suppressing any recirculation zones has been demonstrated. Several ways of improving the process have also been revealed: (i) an increase in the nitrogen flow rate in the shield and a decrease of the curtain flow rate enhance the deposition rate in the outer deposition zone, (ii) a new shield design could bring the INT vein closer to the wafer and increase the deposition rate and thus TEOS conversion. Overall, the results suggest that additional injections of ozone through the shield could help to enhance the deposition rate far from the injector.

Acknowledgements

The authors wish to thank ATMEL (Rousset-France) for its financial support and Professor J.P. Couderc for his valuable contribution.

References

Adachi, M., Okuyama, K., Fujimoto, T., 1997. Film formation by a new chemical vapour deposition process using ionization of tetraethylorthosilicate. Japan Journal of Applied Physics 34 (9A), 1148.

Coltrin, M.E., Ho, P., Moffat, H.K., Buss, R.J., 2000. Chemical kinetics in chemical vapour deposition: growth of silicon dioxide from tetraethoxysylane (TEOS). Thin Solid Films 365, 251–263.

Dobkin, D.M., Mokhtari, S., Schmidt, M., Pant, A., Robinson, L., Sherman, A., 1995. Mechanisms of deposition of SiO_2 from TEOS and related organosilicon compounds and ozone. Journal of Electrochemical Society 142 (7), 2332–2340.

Fujino, K., Nishimoto, Y., Tokumasu, N., Maeda, K., 1990. Silicon dioxide deposition by atmospheric pressure and low temperature CVD using TEOS and ozone. Journal of Electrochemical Society 137 (9), 2883–2887.

Hirschfelder, J.O., Curtiss, C.F., Bird, R.B., 1954. Molecular Theory of Gases and Liquids. Wiley, New York.

Kim, E.J., 1993. Chemical Vapor Deposition of silicon dioxide films from tetraethoxysilane. Ph.D. Thesis, Rensselaer Polytechnic Institute, USA.

Kim, A.J., Gill, W.N., 1994. Modeling of CVD of silicon dioxide using TEOS and ozone in a single wafer reactor. Journal of Electrochemical Society 141 (12), 3462–3472.

Kotani, H., Matsuura, M., Fujini, A., Genjou, H., Nagao, S., 1989. Low temperature APCVD oxide using TEOS-ozone chemistry for multilevel interconnections. International Electron Device Meeting, Technical Digest, IEEE service Center, Piscataway, NJ, USA 669.

Masi, M., Carra, S., Vaccari, G., Crippa, D., 1997. Optimization of SiO_2 atmospheric deposition in continuous belt systems. Electrochemical Society Proceedings 97 (25), 1167–1174.

Nieto, J.P., 2001. Analyse et modélisation d'un réacteur de CVD à fonctionnement continu: application au dépôt de SiO_2 pur et dopé. Ph.D. Thesis, Institut National Polytechnique de Toulouse, France.

Okuyama, K., Fujimoto, T., Hayakashi, T., Adachi, M., 1997. Gas phase nucleation in the tetraethylorthosilicate (TEOS)/O_3 APCVD process. A.I.Ch.E. Journal. 43 (11A), 2688.

Reid, R.C., Prausnitz, J.M., Poling, B.E., 1987. The Properties of Gases and Liquids. fourth ed. McGraw-Hill Book Company, New York.

Saito, K., Uchiyama, Y., Abe, K., 2003. Preparation of SiO_2 films using the Cat-CVD method. Thin Solid Films 430, 287–291.

Watkins, J., 1997. Operating Book WJ1000. Scotts Valley, CA, USA.

Yuan, Z., Mokhtari, S., Ferdinand, A., Eakin, J., Bartholomew, L., 1996. Optimization of SiO_2 film conformality in TEOS/O_3 APCVD. Thin Solid Films 290–291, 422–426.

Zhou, N., Krishnan, A., Kudriatsev, V., Brichko, Y., 1997. Numerical study of TEOS/O_3 CVD mechanisms in an industrial reactor. Fifth International Conference on Advanced Thermal Processing of Semiconductors, RTP'97. New Orleans, LA, USA, pp. 257–268.